by least square regression analysis (Microsoft® Office Excel 2003, Microsoft Corporation, Tokyo).

3. Results

3.1. The amount of ketotifen in PSAs

The amount of ketotifen in PSA-Crystalline and PSA-Amorphous were summarized in Table 2, together with the solubility of the corresponding form of ketotifen per unit area of PSA, which was calculated using the solubility per unit volume of silicone pressure sensitive adhesive matrices measured in our previous study (Inoue et al., 2005) and the thickness of the adhesive layer.

Table 2
The loading amount and solubility of ketotifen in PSAs.

	PSA-Crystalline (nmol/cm^2)	PSA-Amorphous (nmol/cm^2)
Loading amount [a]	370.2	1114.1
Solubility of ketotifen [b]	51.3	520.0

[a] Mean of ten measured values.
[b] Calculated by multiplying the solubility per unit volume (crystalline: 8.06 μmol/cm^3, amorphous: 67.89 μmol/cm^3) and the thickness of the adhesive layer (PSA-Crystalline: 64 μm, PSA-Amorphous: 77 μm).

3.2. In vivo time course of ketotifen amount in PSA, stratum corneum and viable skin tissues during PSA administration

Fig. 1 represents *in vivo* time courses of ketotifen amount in PSA, stratum corneum, and viable skin tissues during the administration of PSA-Crystalline or PSA-Amorphous on the abdominal sites of hairless rats. Ketotifen was constantly released from PSA, and approximately 50% or 80% of loaded ketotifen disappeared, respectively from PSA-Crystalline or PSA-Amorphous after 23-h administration. On the other hand, the amount of ketotifen in the stratum corneum and viable skin tissues were less variable. In order to compare the time course of ketotifen amount in skin tissues between PSA-Crystalline and PSA-Amorphous, they were plotted in Fig. 2 with an extended vertical scale. In the case of PSA-Crystalline, the drug amount in the stratum corneum was initially increased then maintained at almost constant level, while gradual increase was observed in viable skin tissues. On the other hand, in the case of PSA-Amorphous, the drug amount in the stratum corneum and those in viable skin tissues were increased up to 13 h, then gradually decreased. The drug amount shown by PSA-Amorphous at 13 h was at most 2–3 times larger than that of PSA-Crystalline. On the other hand, the drug amount in viable skin tissues shown by PSA-Amorphous reached approximately an 8 times larger level compared to that of PSA-Crystalline.

3.3. Drug release from PSA and transdermal absorption during the administration

Fig. 3a represents the release profile from PSAs. The profile of PSA-Crystalline seems to be almost linear, while slight change was observed in the slope of the profile of PSA-Amorphous at around 7 h and 13 h. The time course of Calculated Transdermal Absorption shown in Fig. 3b suggests approximately 7-h lag time followed by continuous increase up to 23 h for both PSA-Crystalline and PSA-Amorphous. The transdermal absorption rates calculated from the slopes of the profiles between 10 h and 23 h were summarized in Table 3.

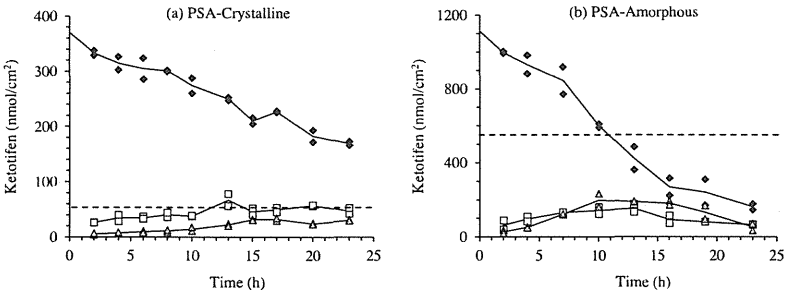

Fig. 1. *In vivo* time course of ketotifen amount in PSA (closed diamond), stratum corneum (open square), and viable skin tissues (gray triangle) during the administration of PSA-Crystalline (a) or PSA-Amorphous (b) on the abdominal sites of hairless rats. Solid lines represent the time course of the mean value. Dashed line represents the solubility of crystalline or amorphous ketotifen per unit area of the corresponding PSA.

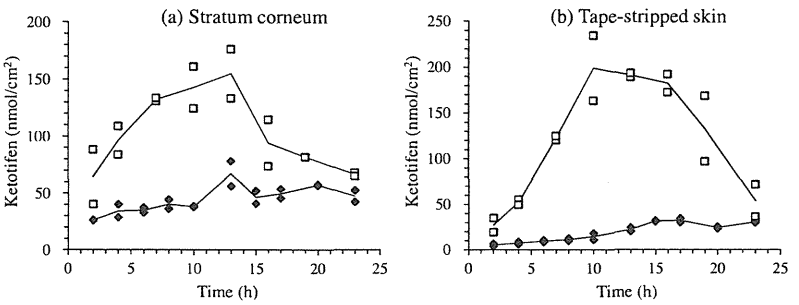

Fig. 2. Comparison of *in vivo* time course of ketotifen amount in the stratum corneum (a) or in viable skin tissues (b) between PSA-Crystalline (closed diamond) and PSA-Amorphous (open square) during the application of PSAs on the abdominal sites of hairless rats. Solid lines represent the time course of the mean value.

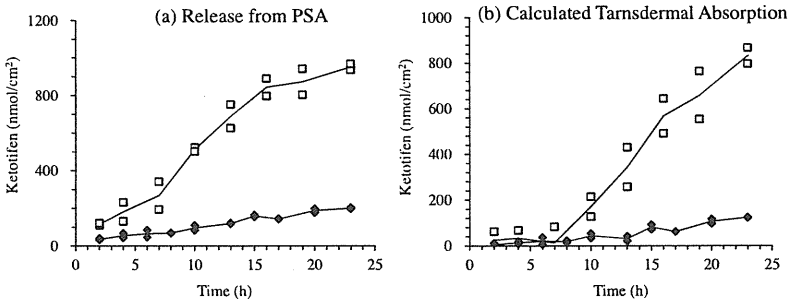

Fig. 3. *In vivo* time course of the release of ketotifen from PSAs (a) and Calculated Transdermal Absorption (b) during the administration of PSA-Crystalline (closed diamond) or PSA-Amorphous (open square) on the abdominal sites of hairless rats. Solid lines represent the time course of the mean value.

Table 3
The *in vivo* transdermal absorption rate or *in vitro* skin permeation rate of ketotifen from PSA-Crystalline or PSA-Amorphous (nmol/h/cm^2).

		PSA-Crystalline	PSA-Amorphous
In vivo	Calculated	6.8[a]	50.8[b]
In vitro	Calculated	9.2[c]	47.6[d]
	Actual	7.4[c]	41.5[d]

[a] Calculated from the slope of the time course between 10 and 23 h.
[b] Calculated from the slope of the time course between 10 and 23 h.
[c] Calculated from the slope of the time course between 8 and 24 h.
[d] Calculated from the slope of the time course between 4 and 17 h.

3.4. In vitro skin permeation

The time course of Actual Skin Permeation and Calculated Skin Permeation *in vitro* were shown in Fig. 4a and b. The time course of Calculated Skin Permeation was similar to Actual Skin Permeation for both PSA-Crystalline and PSA-Amorphous groups. The *in vitro* skin permeation rates were calculated using the slopes of linear portion of profiles and summarized in Table 3. The difference between calculated skin permeation rate and actual skin permeation rate was 24% or 15% respectively for PSA-Crystalline or for PSA-Amorphous, suggesting that *in vivo* transdermal absorption rate can be estimated using the data obtained by subtracting the drug amount in whole skin tissues from the drug release with potential error within 24%. The *in vitro* time course of ketotifen amount in skin tissues was plotted in Fig. 5a and b.

3.5. Time course of ketotifen amount in the stratum corneum and viable skin tissues after the removal of PSA

As shown in Fig. 6, a significant amount of ketotifen was observed in the stratum corneum and in viable skin tissues more than 10 h after the removal of PSA from the skin, suggesting the existence of significant depot in those skin tissues.

4. Discussion

4.1. Enhancement of in vivo transdermal absorption by amorphous form of ketotifen

The enhanced skin permeation of PSA-Amorphous observed in the previous *in vitro* experiments was similarly observed in this study. As shown in Table 3, the degree of the enhancement in the *in vivo* transdermal absorption rate was similar to the degree of the enhancement in the *in vitro* skin permeation rate. This suggests that the mechanism of permeation enhancement induced by amorphous ketotifen observed *in vitro* was equally effective *in vivo*.

4.2. The relationship between the enhancement of transdermal absorption and the drug amount in the skin

As shown in Table 3, the *in vivo* transdermal absorption rate of PSA-Amorphous was approximately 7 times larger than that from PSA-Crystalline. Fig. 2a and b revealed that the drug amount in skin tissues after the administration of PSA-Amorphous was kept at a significantly larger level than that of PSA-Crystalline. These results suggest the correlation between the enhanced transdermal absorption rate obtained by PSA-Amorphous and the increased drug amount in skin tissues. However, there are two points which need further investigation. The first point is that the drug amount in skin tissues shown by PSA-Amorphous was largely fluctuated, while the *in vivo* transdermal absorption rate of PSA-Amorphous seems to be less variable between 7 h and 23 h. The second point is that the ratio of the drug amount in the stratum corneum between PSA-Crystalline and PSA-Amorphous (2–3-fold at maximum) is smaller than the ratio of *in vivo* transdermal absorption (7-fold) despite the

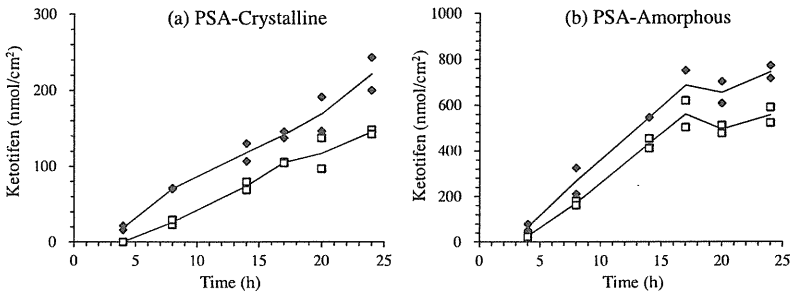

Fig. 4. Comparison of *in vitro* time course of Calculated Skin Permeation (closed diamond) and Actual Skin Permeation (open square) during the application of PSA-Crystalline (a) or PSA-Amorphous (b) on the excised hairless rat skin. Solid lines represent the time course of the mean value.

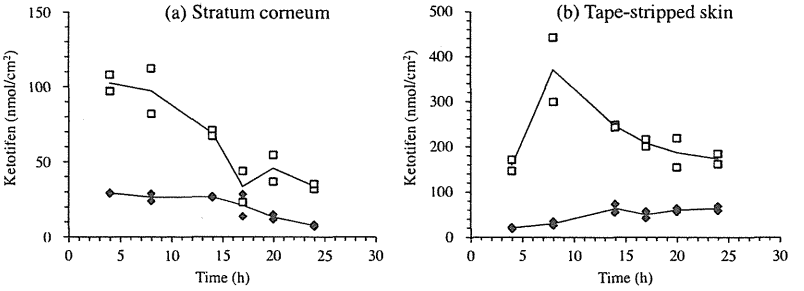

Fig. 5. Comparison of *in vitro* time course of ketotifen amount in the stratum corneum (a) or in viable skin tissues (b) between PSA-Crystalline (closed diamond) and PSA-Amorphous (open square) during the application of PSAs on excised hairless rat skin. Solid lines represent the time course of the mean value.

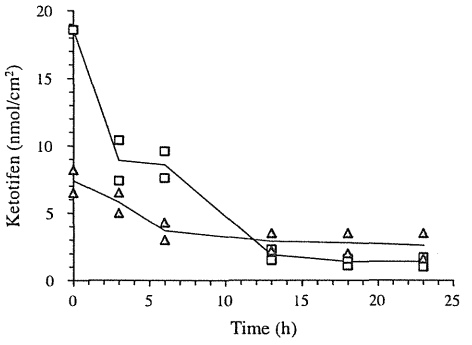

Fig. 6. Time course of ketotifen amount in the stratum corneum (open square) and in the viable skin tissues (gray triangle) after the termination of 4-h transdermal administration of PSA-Crystalline on the abdominal site of hairless rats. Solid lines represent the time course of the mean value.

good coincidence between the drug amount ratio in viable skin tissues (8-fold) and the enhancement of the absorption rate. Even considering the potential error in the procedure to estimate the *in vivo* transdermal absorption as mentioned in Section 3.4, the inconsistency between the enhancement of the transdermal absorption rate and the increase of the drug amount in the stratum corneum is thought to be significant.

Fig. 1 and Table 2 suggest that ketotifen was retained in PSA-Crystalline at a higher level than the solubility during the administration, while the drug content in PSA-Amorphous fell below the solubility after 10 h. This suggests that the supersaturation generated by amorphous ketotifen might be maintained only for the first 10 h followed by gradual decrease due to the drug consumption. The variation of the drug content in skin tissues observed for PSA-Amorphous is probably due to the decline of the driving force for ketotifen transport from the PSA to the stratum corneum.

The inconsistency between the ratio of ketotifen amount in the stratum corneum and the degree of the absorption enhancement was also observed in the *in vitro* data in Fig. 5. They suggest a non-linear relationship between the permeation and partition in the stratum corneum. Many drugs have been reported to have the ability to bind keratin protein in the stratum corneum, and this property is thought to lead to differences in the effective and true diffusion and partition coefficients, a retardation of the absorption process, and a sustained presence of the bound compound in the tissue (Hansen et al., 2011). Our previous study also suggested that the delipidized domain (mainly consists of keratin) contributes to approximately 40% of the total capacity for ketotifen partition in the stratum corneum, while the main permeation pathways of ketotifen are located in the lipid domain (Inoue et al., 2000). One possible mechanism to cause a non-linear relationship between the permeation and partition observed in PSA-Amorphous could be the combination of the small contribution of bound ketotifen to the permeability and the saturation phenomena in the binding of ketotifen to the keratin domain when excess ketotifen is applied. Verification of this assumption is a subject of future study.

4.3. Duration of the enhanced transdermal absorption

Despite the short duration in maintaining the drug content above the solubility, the transdermal absorption rate from PSA-Amorphous was kept at fairly constant level for up to 23 h. This may be due to the depot effect of the skin tissues. Fig. 6 shows that significant amount of ketotifen was retained in skin tissues even 10 h after the removal of PSA, suggesting that the effect of the drug concentration change in PSA on the transdermal absorption can be masked or delayed by the drug absorption from the skin depot into systemic circulation for a while.

5. Conclusion

Enhanced transdermal absorption of ketotifen by PSA-Amorphous was observed *in vivo* similarly to the enhanced skin permeation observed *in vitro*, and good coincidence was observed between the enhancement factor and the increase of drug amount in viable skin tissues. The increase of drug amount in the stratum corneum was not consistent with the degree of the absorption enhancement probably due to a non-linear relationship between the permeability and partition in the stratum corneum. PSA-Amorphous used in this study could maintain a constant supersaturated level only for 10 h, but probably due to the depot effect of skin tissues, constant absorption rate could be maintained at least for 23 h. These results suggest the usefulness of the amorphous form to obtain enhanced and prolonged transdermal delivery of ketotifen.

References

Hansen, S., Selzer, D., Schaefer, U.F., Kasting, G.B., 2011. An extended database of keratin binding. J. Pharm. Sci. 100 (5), 1712–1726.
Inoue, K., Ogawa, K., Suzuki, Y., Okada, J., Kusai, A., Ikeda, M., Nishimura, K., 2000. The skin permeation mechanism of ketotifen: evaluation of permeation pathways and barrier components in the stratum corneum. Drug Dev. Ind. Pharm. 26 (1), 45–53.
Inoue, K., Ogawa, K., Okada, J., Sugibayashi, K., 2005. Enhancement of skin permeation of ketotifen by supersaturation generated by amorphous form of the drug. J. Cont. Rel. 108, 306–318.
Kim, J.H., Choi, H.K., 2002. Effect of additives on the crystallization and the permeation of ketoprofen from adhesive matrix. Int. J. Pharm. 236, 81–85.
Mallick, S., Pattnaik, S., Swain, K., De, P.K., Saha, A., Ghosal, G., Mondal, A., 2008. Formation of physically stable amorphous phase of ibuprofen by solid state milling with kaolin. Eur. J. Pharm. Biopharm. 68, 346–351.
McCarley, K.D., Bunge, A.L., 2001. Pharmacokinetic models of dermal absorption. J. Pharm. Sci. 11, 1699–6719.

Moser, K., Kriwet, K., Naika, A., Kalia, Y.N., Guy, R.H., 2001. Passive Skin penetration enhancement and its quantification *in vitro*. E. J. Pharm. Biopharm. 52, 103–112.

Pellet, M.A., Hadgraft, J., Davis, A.F., 1994. The permeation of solutions of piroxicam across silicon membranes and human skin *in vitro*. Int. J. Pharm. 111, 1–6.

Pellet, M.A., Castellano, S., Hadgraft, J., Davis, A., 1997. The permeation of solutions of piroxicam across silicon membranes and human skin *in vitro*. J. Control. Release 46, 205–217.

Raghavan, S.L., Trividic, A., Davis, A.F., Hadgraft, J., 2001. Crystallization of hydrocortisone acetate: influence of polymers. Int. J. Pharm. 212, 213–221.

Schwarb, F.P., Imanidis, G., Smith, E.W., Haigh, J.M., Surber, C., 1999. Effect of concentration and degree of saturation of topical fluocinonide formulations on *in vitro* membrane transport and in vivo availability on human skin. Pharm. Res. 16, 909–915.

Pharm Res (2012) 29:2477–2488
DOI 10.1007/s11095-012-0777-6

RESEARCH PAPER

Effect of Direction (Epidermis-To-Dermis and Dermis-To-Epidermis) on the Permeation of Several Chemical Compounds through Full-Thickness Skin and Stripped Skin

Takeshi Oshizaka • Hiroaki Todo • Kenji Sugibayashi

Received: 30 November 2011 / Accepted: 11 May 2012 / Published online: 24 May 2012

ABSTRACT

Purpose Compound permeation through stratum corneum-stripped skin is generally greater than that through full-thickness skin. In addition, epidermis-to-dermis permeation profile should be the same as dermis-to-epidermis permeation profile. However, stripped skin permeability of some compounds was lower than full-thickness skin permeability and different permeabilities were found for some compounds between the two directions of skin permeation. The reasons for these findings were investigated in this study.

Methods Full-thickness or stripped hairless rat skin was set in a Franz-type diffusion cell, and a solution of compound was applied on the epidermis or dermis side to determine the *in vitro* skin permeability.

Results Although the stripped skin permeability of pentyl paraben (PeP) with extremely high $\log K_{o/w}$ was lower than full-thickness skin permeabilities, the addition of 3% ethanol resulted in the expected permeation order. Epidermis-to-dermis permeation of PeP through full-thickness skin was higher than dermis-to-epidermis permeation. Epidermis-to-dermis permeations of fluorescein isothiocyanate dextran (FD-4) and isosorbide 5-mononitrate with negative $\log K_{o/w}$ were also higher than those in the opposite direction.

Conclusions Morphological observation of skin after FD-4 permeation suggested that a conically shaped trans-follicular permeation pathway model could be advocated to explain the difference between the epidermis-to-dermis permeation and that in the opposite direction.

T. Oshizaka • H. Todo • K. Sugibayashi (✉)
Faculty of Pharmaceutical Sciences, Josai University
1-1 Keyakidai
Sakado, Saitama 350-0295, Japan
e-mail: sugib@josai.ac.jp

KEY WORDS conical pore permeation model · hair follicle · interfacial resistance · permeation direction · skin permeation

INTRODUCTION

Many topical formulations containing many pharmaceutical additives in addition to therapeutically active compounds have been designed. Since such additives may have undesirable effects, skin permeation studies are very important for safety evaluation as well as effectiveness assessment. Measurement of skin permeability has been found to be difficult in *in vivo* experiments as well as *in vitro* experiments using human skin. The latter is due to the low availability and high variability of human skin. Many researchers have used hairless rat skins and pig skins owing to the high correlation between compound or chemical permeations through these skins and those through human skin (1–5). Although animal experiments have been widely undertaken, the concept of animal welfare and the 3Rs of animal experiments limit these experiments and necessitate alternatives (6–9). Understanding the skin permeation properties and the mechanism of action of compounds and chemical compounds is very important to establish alternatives to animal experiments.

Most of the permeation profiles of compounds through skin reflect kinetic processes that can be explained by Fick's law of diffusion. Generally, the uppermost layer of skin, stratum corneum, is the biggest barrier against compound entry through the skin (10–13). Since the stratum corneum consists of several layers of dead cells, corneocytes, transporters and metabolic enzymes were thought to contribute little to the skin permeation of most compounds. Thus, material permeation through full-thickness skin should be lower than that through stratum corneum-stripped skin. In addition, epidermis-to-dermis permeation should be the

same as dermis-to-epidermis permeation, even though the outer and inner surfaces are quite different as most likely is the interaction between the permeant and these two different biological tissues. In our preliminary experiments, the stripped skin permeability of some compounds was lower than the full-thickness permeability and different permeabilities of some compounds were found between the two directions of skin permeation. Parabens (methyl, ethyl, *n*-propyl, *n*-butyl, and *n*-pentyl parabens), isosorbide 5-mononitrate (ISMN), and fluorescein isothiocyanate dextran (FD-4) were used as model penetrants. Full-thickness and stripped skin samples excised from male hairless rats were used as skin membrane. Several *in vitro* skin permeation studies were conducted using Franz-type diffusion cells to evaluate diffusion and permeation profiles through the skin and to obtain morphological information on the permeation pathway.

Theory of Skin Permeation

Figure 1a and b illustrate concentration-distance profiles of compounds applied through full-thickness skin and stripped skin, respectively, in a steady state condition. Full-thickness skin consists of stratum corneum layer and underlying epidermis and dermis, which can be expressed by a 2-layered diffusion model, whereas stripped skin alone can be expressed by a one-layered diffusion model (14–16). Since the stratum corneum is the biggest barrier to the skin permeation of chemical compounds, as mentioned above, the permeation rate through full-thickness skin (Fig. 1a) is generally lower than that through stripped skin (Fig. 1b).

Figure 1c and d show a comparison of diffusion models of epidermis-to-dermis permeation (Fig. 1c) and dermis-to-epidermis permeation (Fig. 1d), where Fig. 1c is the equivalent of Fig. 1a. Unless no skin adsorption, no skin metabolism, and no transporter-mediated permeation occur in passive skin permeation, epidermis-to-dermis permeation should be exactly the same as dermis-to-epidermis permeation of chemical compounds.

Let us explain that the epidermis-to-dermis permeation through full-thickness skin is the same as the dermis-to-epidermis permeation. The abscissa in Fig. 1 shows the direction of the membrane permeation, and the width of the skin shows the thickness of the skin, whereas the axis of the ordinate represents the concentration of the penetrant applied on the skin. Hatched areas in the figures show the amount of penetrants in unit area of skin (usually presented as $\mu g/cm^2$), and products of concentration slopes in the stratum corneum and viable epidermis/dermis (*i.e.* concentration gradient) and diffusion coefficient of compounds become the permeation rate of compounds through the membrane. Two examples (one is a lipophilic compound and the other is a hydrophilic compound) are shown to explain that no difference is found between the epidermis-to-dermis and the dermis-to-epidermis permeation rates. When the partition coefficient of a lipophilic compound from the vehicle to stratum corneum is 4.0 and that from the vehicle to viable epidermis and dermis is unity (1.0), the partition coefficient from the stratum corneum to the viable epidermis/dermis must be 1/4, and that in the opposite direction is 4.0. In addition, the resistant ratio of stratum corneum against full-thickness skin is considered to be 0.8 (resistant ratio of viable epidermis and dermis against full-thickness skin is 0.2). Furthermore, compound concentration in the vehicle is considered to be 1.0, and sink condition is maintained in the receiver side. Then, the concentration gradient of penetrant across the stratum corneum becomes $16/5/L_{sc}$ and that across the viable epidermis and dermis is $1/5/L_{ved}$ for both directions, as illustrated in Fig. 1c and d. Thus, the same skin permeation rates must be obtained for the two directions since the concentration gradient is the same.

Let us explain in case of a hydrophilic compound having a partition coefficient from the vehicle to stratum corneum is 2.0 and that from the vehicle to viable epidermis and dermis is unity (1.0) as the same as above, the partition coefficient from the stratum corneum to the viable epidermis/dermis become 1/2, and that in the opposite direction is 2.0. The resistant ratio of stratum corneum against full-thickness skin is considered to be 0.95 (resistant ratio of viable epidermis and dermis against full-thickness skin is 0.05). The same compound concentration in the vehicle (1.0) applied under a sink condition in the receiver side. Then, the concentration gradient of penetrant across the stratum corneum becomes $19/10/L_{sc}$ and that across the viable epidermis and dermis is $1/20/L_{ved}$ for both directions, as illustrated in Fig. 1e and f. Thus, the same skin permeation rates must be obtained for the two directions for a hydrophilic compound.

In the case of stripped skin permeation both for a lipophilic compound and hydrophilic compound, a one-layered model is applied to explain the permeation profile. Thus, it is easy to understand that the epidermis-to-dermis permeation should be the same as the dermis-to-epidermis permeation.

In contrast, the steady state concentration for a lipophilic and hydrophilic compound in skin in the case of epidermis-to-dermis permeation is 0.33 and 0.1275 and that in dermis-to-epidermis permeation is 0.97 and 0.9725, respectively, when the thicknesses of stratum corneum and viable epidermis/dermis are 1 and 9. Thus, skin concentration differs between the cases of epidermis-to-dermis permeation and dermis-to-epidermis permeation both for lipophilic and hydrophilic compounds. Even when the other ratios were used, the calculated epidermis-to-dermis permeation of compounds must be the same to the dermis-to-epidermis permeation, but full-thickness skin concentration of the compounds after application to the dermis side is not the same to that to the epidermis side.

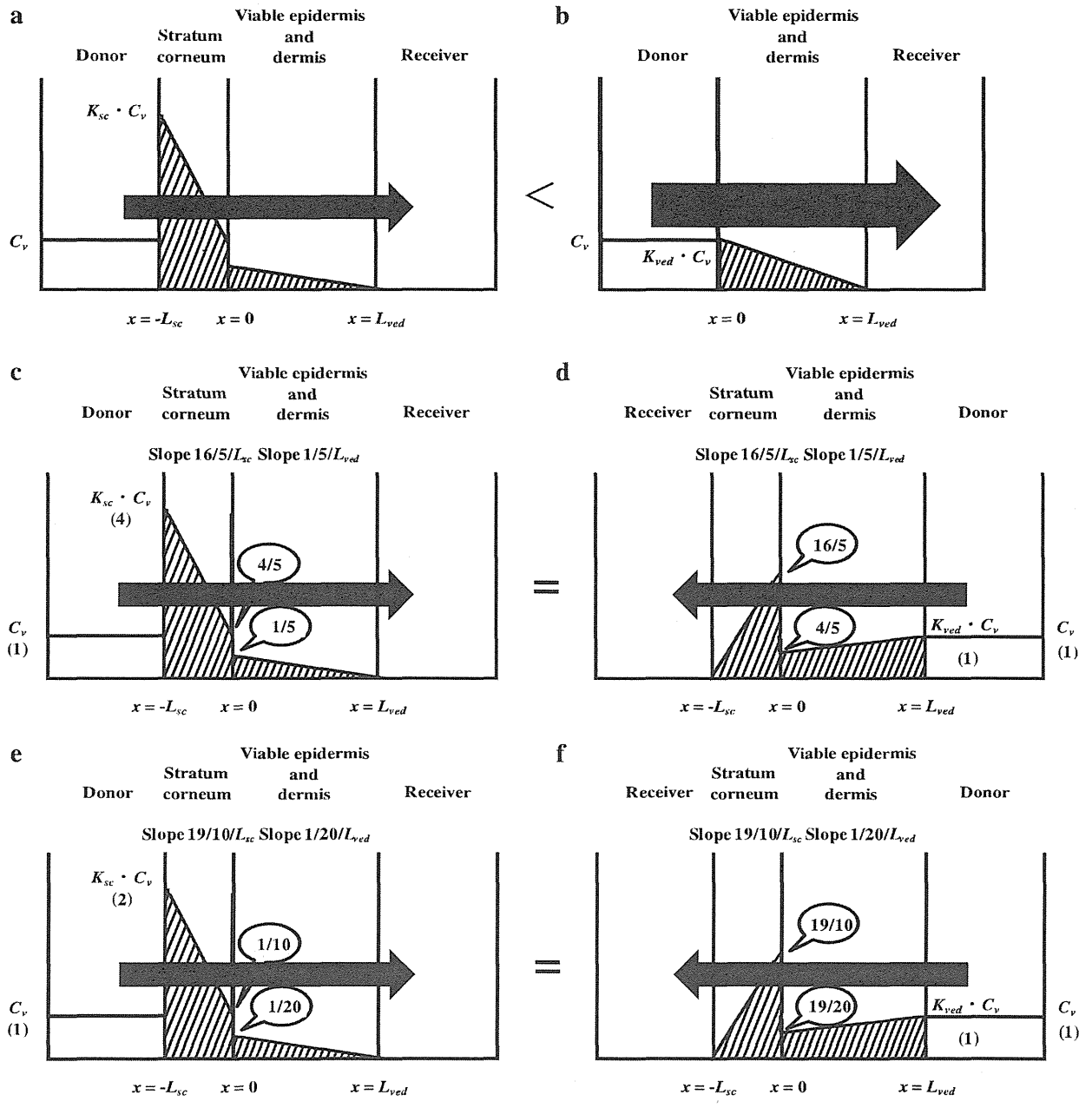

Fig. 1 Concentration-distance profile showing permeation profiles of compound through full-thickness skin (**a**) and stripped skin (**b**), and that showing full-thickness skin permeation profiles of a lipophilic and hydrophilic compound in epidermis-to-dermis (**c**, **e**) and dermis-to-epidermis directions (**d**, **f**). Width of arrows corresponds to skin permeation rate.

MATERIALS AND METHODS

Reagents and Materials

Model penetrants: methyl paraben (MP), ethyl paraben (EP), *n*-propyl paraben (PP), *n*-butyl paraben (BP), *n*-pentyl paraben (PeP), and isosorbide 5-mononitrate (ISMN), were purchased from Tokyo Chemical Industry Co., Ltd. (Tokyo, Japan). Fluorescein isothiocyanate dextran with an average molecular weight of 4.4 kDa (FD-4) was obtained from Sigma Aldrich (St. Louis, MO, U.S.A.). Table I shows a summary of molecular weights (*M.W.*) and logarithmic values of *n*-octanol/water partition coefficients ($\log K_{o/w}$) of these model compounds. Diisopropyl fluorophosphate (DFP), an esterase inhibitor, was obtained from Wako Chemical Industries, Ltd. (Osaka, Japan). Other chemicals and reagents were

of special grade or HPLC grade commercially obtained and used without further purification.

Experimental Animals

Male hairless rats (WBN/IL-Ht strain) weighing 220 to 260 g were obtained from Life Science Research Center, Josai University (Sakado, Saitama, Japan), or Ishikawa Experimental Animal Laboratories (Fukaya, Saitama, Japan). The rats were kept in an animal room where the temperature was maintained at 25±2°C and light was on from 7:00 to 19:00. Food and water were provided *ad libitum*. All animal feeding and experiments were approved by the Institutional Animal Care and Use Committee of Josai University.

Human scalp was purchased from Biopredic International (Rennes, France). The donor was a 60-year-old Caucasian lady. The average thickness of the skin was 4 mm. This human experiment was approved by and followed the guidelines on the ethical use of human-origin organs and tissues of KAC Co., Ltd. (Ritto, Shiga, Japan).

In Vitro Skin Permeation Experiments

Abdominal skin was cleaned using wet Kimwipe and excised from hairless rats under anesthesia by *i.p.* injection of pentobarbital (50 mg/kg). Stripped skin was made by stripping off the stratum corneum 20 times using adhesive tape and excised. To decrease the variability in skin permeability due to abdominal sites of skin, only right and left upper abdominal skin was used. The excess fat was trimmed off from the excised skin, and the skin sample was set in a Franz-type diffusion cell (effective diffusion area, 1.77 cm^2) in which the receiver chamber was warmed at 32°C. Compound solution and PBS were added to the cap cell and receiver cell, respectively, in all permeation experiments. Skin piece was mounted in the diffusion cell with the epidermis side facing upwards in the epidermis-to-dermis permeation experiment, whereas the dermis side facing upwards in the dermis-to-epidermis permeation experiment. DFP in pH7.4 phosphate-buffered saline (PBS) at a concentration of 2.7 μmol/mL (6 mL) was added to the receiver chamber and maintained for 30 min to reduce metabolism of parabens. Then, the skin permeation experiments were started. No effect of DFP was confirmed on the skin permeation of parabens and other compounds (17–19). In the cases of other penetrants, only PBS was used for pretreatment. A penetrant solution in PBS or 3% ethanol (0.5 or 1.0 mL) was added to the donor chamber, whereas DFP in PBS (0.54 μmol/mL) or PBS alone (6 mL each) was added to the receiver chamber to start the permeation experiments. The concentration of each penetrant applied was as follows: MP, 1520 μg/mL; EP, 500 μg/mL; PP, 200 μg/mL; BP, 100 μg/mL; PeP, 50 μg/mL; FD-4, 1 mg/mL; and ISMN, 100 mg/mL. Receiver solution was agitated using a stirrer bar and a magnetic stirrer throughout the experiments. An aliquot (500 μL) was withdrawn from the receiver chamber and the same volume of PBS was added to the chamber to keep the volume constant. Penetrant concentration in the receiver chamber was determined by HPLC or using a fluorescence spectrophotometer.

Hair on the human scalp was carefully cut using scissors. The resulting scalp was cleaned using PBS and set in a Franz-type diffusion cell. Skin permeation experiment was carried out after 12-h hydration with PBS.

Table I Physical Properties of Model Compounds

	MP	EP	PP	BP	PeP	FD-4	ISMN
M.W.	152.2	166.1	180.2	194.2	208.3	4400	191.1
$\log K_{o/w}$ [a]	1.93	2.27	2.81	3.53	4.10	−0.773	−0.151

[a] *n*-Octanol/water partition coefficient at 37°C

Determination of Extraction Ratio

The withdrawn sample containing parabens (200 μL) was mixed with 200 μL acetonitrile containing internal standard (EP for MP, MP for EP, BP for PP, PP for BP, and BP for PeP) and centrifuged at 4°C for 5 min. The obtained supernatant was injected into an HPLC system. The HPLC system (Shimadzu, Japan) consisted of a system controller (CBM-20A), a pump (LC-20 AD), an auto-sampler (SIL-20 AC), a column oven (CTO-20A), a UV detector (SPD-M20A), and analysis software (LC Solution). The column was LiChroCART® 250–4 (KGaA, 64271; Merck, Darmstadt, Germany) maintained at 40°C. Mobile phases were as follows: MP and EP, 0.1% phosphoric acid:acetonitrile (65:35); PP and BP, 0.1% phosphoric acid:acetonitrile (55:45); and PeP, 0.1% phosphoric acid:acetonitrile (45:55). The flow rate was adjusted to 1.0 mL in each case. The injection volume of sample was 20 μL and detection was carried out at UV 260 nm.

The ISMN sample was mixed with the same volume of acetonitrile and centrifuged as explained above. An absolute calibration method was used. The column was Inertsil® ODS-34.6 mm×150 mm (GL Sciences Inc., Japan), the mobile phase was water:acetonitrile (9:1), and detection was carried out at UV 220 nm. Other methods are the same as above for the paraben assay.

FD-4 was determined using a fluorescence spectrophotometer (RF-5300PC; Shimadzu, Japan) at the emission and excitation wavelengths of 490 and 520 nm, respectively.

Sectioning of Frozen Skin

Skin sectioning was done only after permeation experiment FD-4. After the permeation experiment, the skin surface was washed twice using 1 mL of PBS on the Franz-type diffusion cell. The skin sample taken from the diffusion cell was

vertically cut at 0.2 mm thickness using a razor blade, embedded in super cryoembedding medium (Leica Microsystems, Tokyo, Japan), and frozen in dry iced isopentane. Skin slices (10 μm in thickness) were made using a cryostat (CM3050S, Leica Microsystems). Each skin slice was observed under a confocal laser scanning microscope (Fluoview FV1000 and software: FV10-ASW, Olympus, Japan).

RESULTS

Figure 2 shows the time course of the cumulative amounts of parabens that permeated through full-thickness skin and stripped skin. An esterase inhibitor, DFP, was used in the skin permeation experiments of parabens. Therefore, metabolite of parabens, *p*-hydroxybenzoic acid, was not found in the receiver cells. We then ignored the effect of metabolism of parabens on the skin permeation. It was confirmed that the use of DFP did not affect the barrier function of skin (17–19). Each profile in the figure shows the typical lag time period and following steady state flux. The slopes in case of MP and EP gradually decreased with time. This was due to a decrease in donor concentration. As expected, stripped skin permeabilities were higher than full-thickness skin permeabilities of MP to PP with log$K_{o/w}$ of 1.93 to 2.81 (Fig. 2a-c). On the other hand, the stripped skin permeation

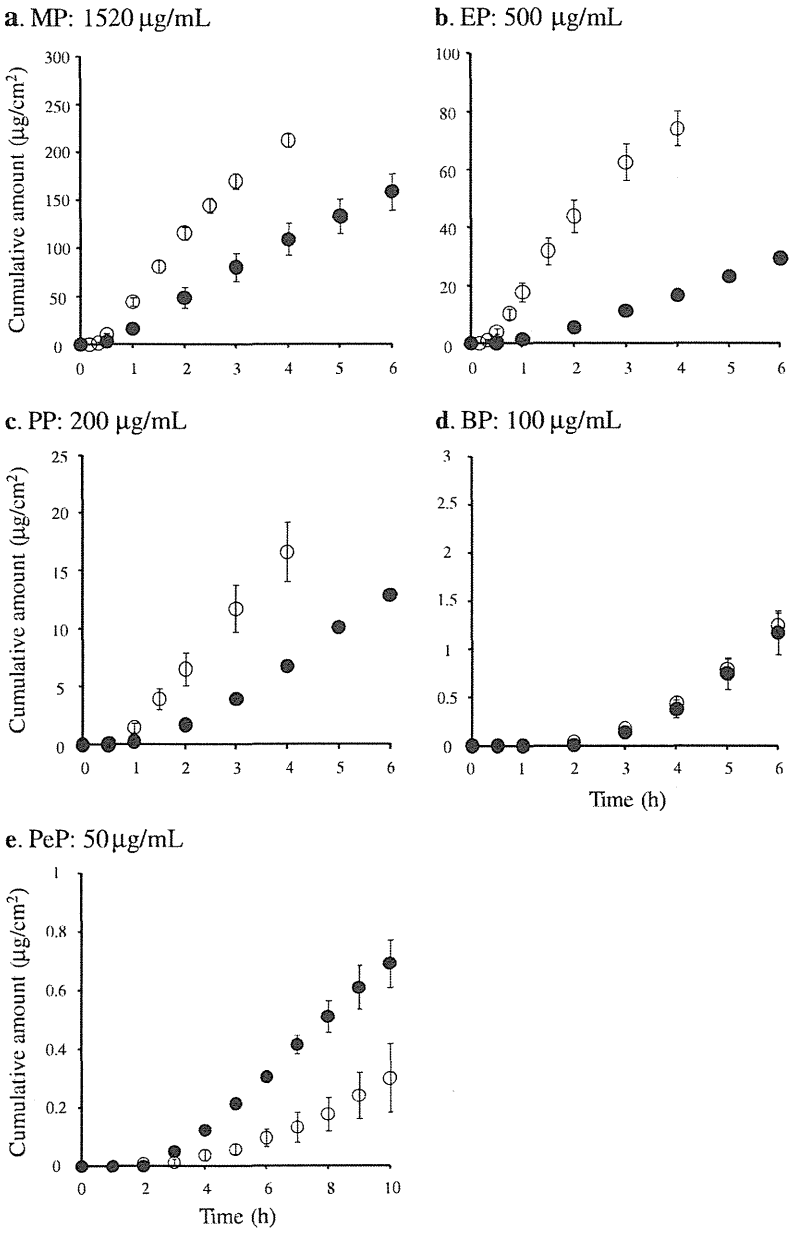

Fig. 2 Time course of changes in the cumulative amount of parabens that permeated through hairless rat skin. Symbols: through full-thickness skin from PBS (●), through stripped skin from PBS (○). Data are shown as the mean ± S.E. (n=3–5).

of BP ($\log K_{o/w}$, 3.53) was almost the same as the full-thickness skin permeation of the compound (Fig. 2d). Thus, low-molecular-weight compounds with a $\log K_{o/w}$ value greater than 3.53 easily permeate through the lipophilic membrane, stratum corneum, and the overall permeation is limited by the viable epidermis/dermis barrier rather than the stratum corneum barrier. Interestingly, stripped skin permeation of PeP was lower than the full-thickness skin permeation, as shown in Fig. 2e. Since the skin barrier consists of a barrier in the stratum corneum and one more barrier in the viable epidermis/dermis, almost the same permeation may be obtained for the BP permeation (Fig. 2d), but higher permeation through full-thickness skin than that through stripped skin is not possible as in PeP permeation (Fig. 2e).

We considered that this was due to interfacial migration resistance occurring or an unstirred diffusion layer forming between the bulk donor solution and the skin membrane (20–26). Theoretically, partition or distribution of penetrants immediately takes place from the vehicle to the skin at the beginning of the skin permeation (27). When interfacial resistance or unstirred layer is not negligible, the partition or distribution of penetrants from the vehicle to the skin develops a kinetic profile in the skin permeation profile. Since the effect of interfacial resistance or unstirred layer may be reduced by an increase in the affinity of skin to the donor solution, 3% ethanol was used instead of PBS. Skin permeation experiment of PeP was performed and that of MP was also carried out for comparison.

Figure 3 shows the results. MP permeations through both full-thickness skin and stripped skin from PBS were the same as those from 3% ethanol (Fig. 3a). Although ethanol was found to have an enhancing effect on the skin permeation of many compounds, 3% ethanol did not have any enhancing effect, probably due to the low concentration of ethanol. In contrast, PeP permeation from 3% ethanol through stripped skin was not significantly ($p>0.05$) different from that through full-thickness skin (Fig. 3b), although the compound permeation from PBS had an unusual result, as shown in Fig. 2e.

As mentioned above, the use of 3% ethanol increased the affinity between the compound vehicle and the skin surface to decrease the effect of permeation resistance or an unstirred diffusion layer on the delayed skin permeation (20–26). Similar permeations of PeP ($\log K_{o/w}$, 4.1) even from 3% ethanol through stripped skin and full-thickness skin mean a greater contribution of the viable epidermis/dermis barrier to the total skin barrier.

As the main focus in the present study, the reason for the difference between epidermis-to-dermis permeation and dermis-to-epidermis permeation of compounds was evaluated. Figure 4a and b show the time course of the cumulative amount of PeP that permeated through skin from PBS and 3% ethanol, respectively. When PBS was used in the donor and receiver chambers, the epidermis-to-dermis permeation through full-thickness skin was higher than the dermis-to-epidermis permeation through full-thickness skin, epidermis-to-dermis permeation through stripped skin, and dermis-to-epidermis permeation through stripped skin. In addition, the latter three cases showed almost the same permeation. Interfacial resistance or unstirred diffusion layer may be the reason for these results (20–26). Then, 3% ethanol was used in the donor and receiver solutions, which resulted in no change in the skin permeation for the two directions.

Therefore, the interfacial resistance or unstirred diffusion layer probably affects the skin permeation of PeP. Since the PeP permeation was decreased through viable epidermis and dermis in the present study, the interfacial resistance or unstirred diffusion layer probably affects the stripped skin permeation. The reason for no interfacial effect being observed on the full-thickness skin permeation was the high affinity of PeP to the highly lipophilic stratum corneum.

Figure 5 shows the time course of the cumulative amount of MP permeated through skin from PBS and 3% ethanol solution. Almost the same stripped skin permeation of MP was observed from PBS. Through the full-thickness skin from PBS, however, the epidermis-to-dermis permeation of MP was higher than the dermis-to-epidermis permeation. Ethanol solution at a concentration of 3% was used instead

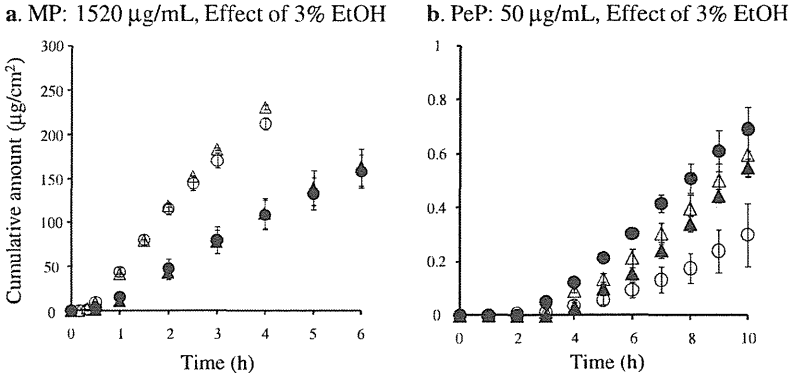

Fig. 3 Time course of changes in the cumulative amounts of MP (**a**) and PeP (**b**) that permeated through hairless rat skin. Symbols: through full-thickness skin from PBS (●), through stripped skin from PBS (○), through full-thickness skin from 3% ethanol (▲), through stripped skin from 3% ethanol (Δ). Data are shown as the mean ± S.E. (n=3–5).

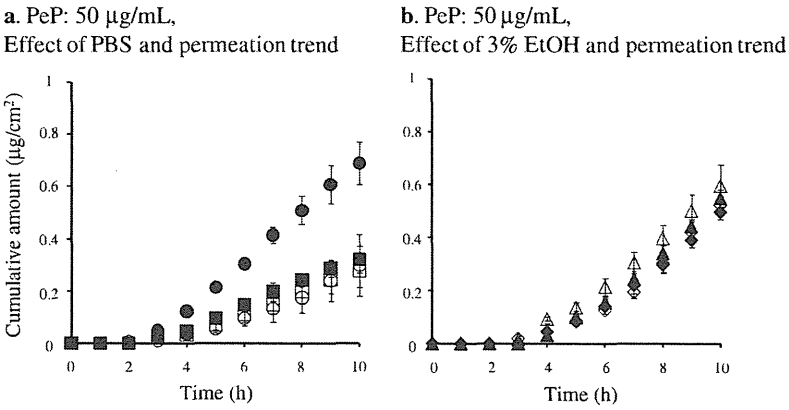

Fig. 4 Time course of changes in the cumulative amount of PeP that permeated through hairless rat skin from PBS (**a**) and 3% ethanol (**b**). Symbols: full-thickness skin permeation in the epidermis-to-dermis direction from PBS (●), stripped skin permeation in the epidermis-to-dermis direction from PBS (○), full-thickness skin permeation in the dermis-to-epidermis direction from PBS (■), stripped skin permeation in the dermis-to-epidermis direction from PBS (□), full-thickness skin permeation in the epidermis-to-dermis direction from 3% ethanol (▲), stripped skin permeation in the epidermis-to-dermis direction from 3% ethanol (Δ), full-thickness skin permeation in the dermis-to-epidermis direction from 3% ethanol (♦), stripped skin permeation in the dermis-to-epidermis direction from 3% ethanol (◊). Data are shown as the mean ± S.E. (n=3–5).

of PBS to overcome the effect of interfacial resistance or unstirred layer. The same trends (higher epidermis-to-dermis permeation through full-thickness skin) were observed. The same permeability was observed from 3% ethanol solution and PBS, suggesting that no interfacial resistance took place. Active transport or the effect of transporters could have been involved in skin permeation (28,29). However, it appears that transporters were not involved in skin permeation of MP because the epidermis-to-dermis permeation through viable skin (stripped) was the same as the dermis-to-epidermis permeation. Next, the final donor concentration was determined and the permeation data were modified to take account of the adsorption of MP on the diffusion cell and skin surface (30,31). The obtained results are shown in Fig. 6. Normalized cumulative amount (% dose applied/cm^2) is used in this figure. No difference was found in the two directions of permeation of MP through full-thickness skin, suggesting that MP must be easily adsorbed or distributed on the skin surface or glass diffusion cell.

Next, the effect of direction was investigated for the skin permeation of aqueous compounds. Figures 7a and b show the time courses of the cumulative amounts of FD-4 and ISMN, respectively, which permeated through full-thickness skin. Epidermis-to-dermis permeations through stripped skin of FD-4 and ISMN were the same as dermis-to-epidermis permeations, which was similar to the case for MP (data not shown). In contrast, the epidermis-to-dermis permeations through the full-thickness skin of FD-4 and ISMN were both higher than the dermis-to-epidermis permeations. We then modified data by the final concentration in the donor solution. The results are shown in Fig. 7c and d. Normalized cumulative amount (% dose applied/cm^2) was also used for the figure the same as in Fig. 6. Different permeabilities were still observed between the epidermis-to-dermis and dermis-to-epidermis permeations.

We considered that the reason for this might be the morphological shape of the permeation pathway through skin, especially for the high-molecular-weight hydrophilic compound, FD-4. Skin permeation of chemical compounds of more than 500 Daltons is severely limited (32). Although FD-4 has a molecular weight about 9-times greater then 500

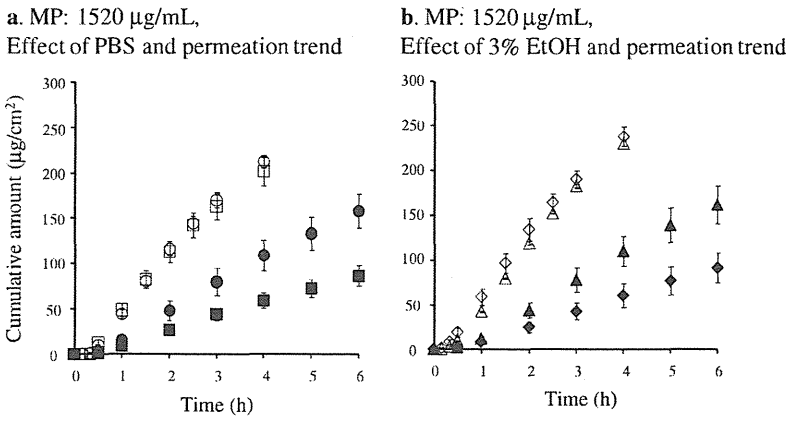

Fig. 5 Time course of changes in the cumulative amount of MP that permeated through hairless rat skin from PBS (**a**) and 3% ethanol (**b**). Symbols: as in Fig. 4. Data are shown as the mean ± S. E. (n=3).

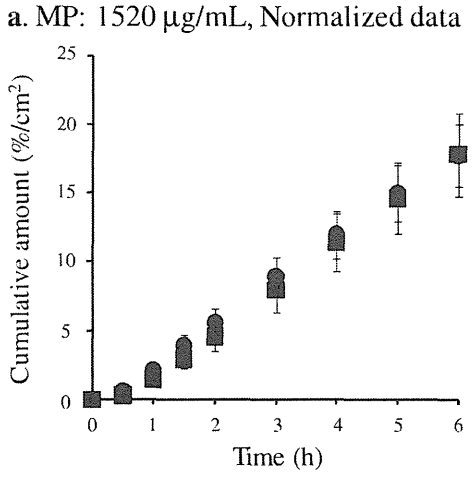

Fig. 6 Time course of changes in the normalized cumulative amount of MP that permeated through hairless rat skin. Symbols: as in Fig. 4. Data are shown as the mean ± S.E. (n=3).

Daltons, skin permeation of FD-4 was still measurable. In contrast, skin permeation of FD-4 through a three-dimensional cultured human skin model, LSE-high, could not be observed (33). This may be due to the lack of hair follicles in the cultured skin model. Figure 8 shows the morphological findings of a skin slice. The skin sample was obtained after the permeation experiment for FD-4. Figure 8a shows the skin slice after the epidermis-to-dermis permeation experiment. No fluorescence was observed in the stratum corneum, whereas low fluorescence was found in the hair follicles. On the other hand, Fig. 8b shows the view after the dermis-to-epidermis permeation experiment. No fluorescence was observed in the stratum corneum, but low fluorescence was observed in the hair follicles and viable epidermis and dermis. These results suggest that the primary permeation pathway for FD-4 must be the hair follicles. By megascopic observation (data not shown), an obvious trail of fluorescence was found on the FD-4 permeation in the sample for epidermis-to-dermis permeation, whereas no

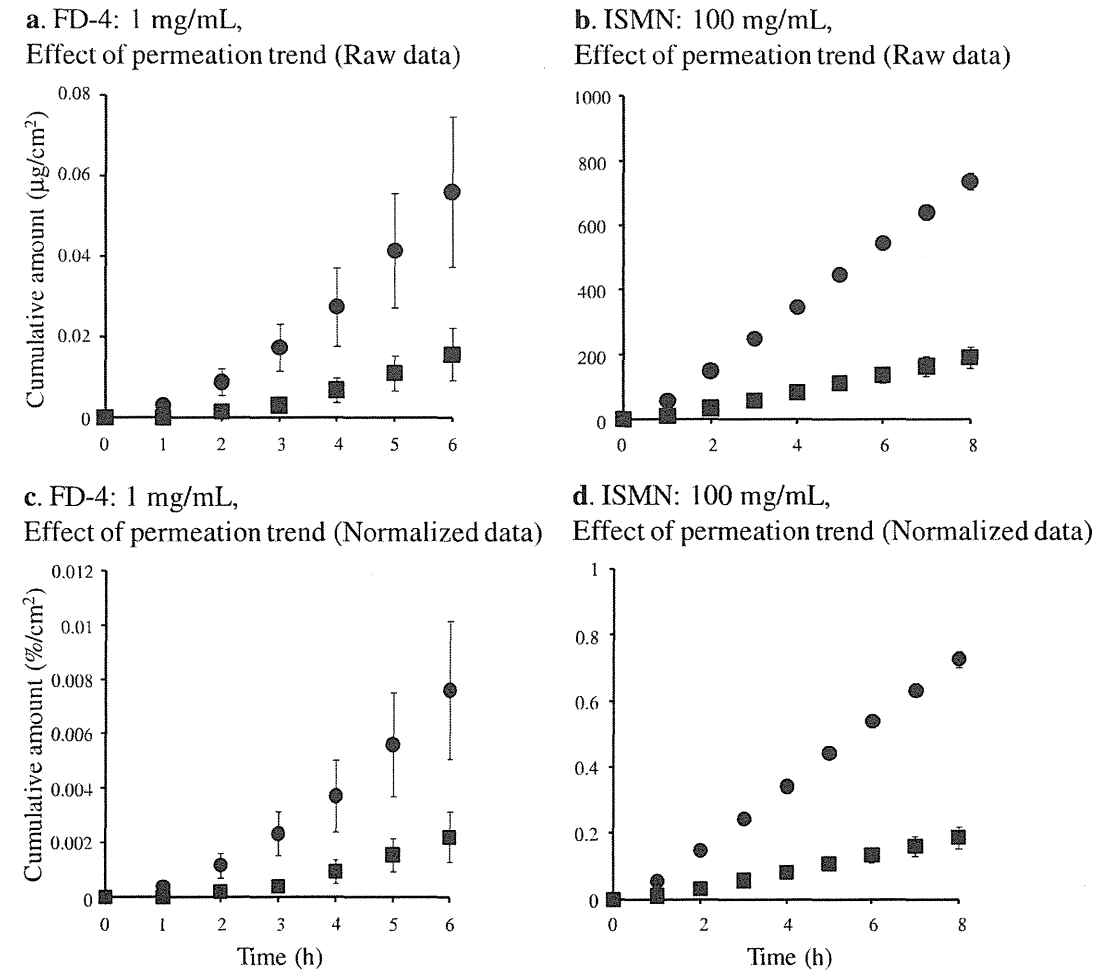

Fig. 7 Time course of changes in the cumulative amounts of FD-4 (**a**, **c**) and ISMN (**b**, **d**) permeated through full-thickness skin. (**a**, **b**) Raw data (μg/cm²), and (**c**, **d**) normalized data (%/cm²). Symbols: as in Fig. 4. Data are shown as the mean ± S.E. (n=3).

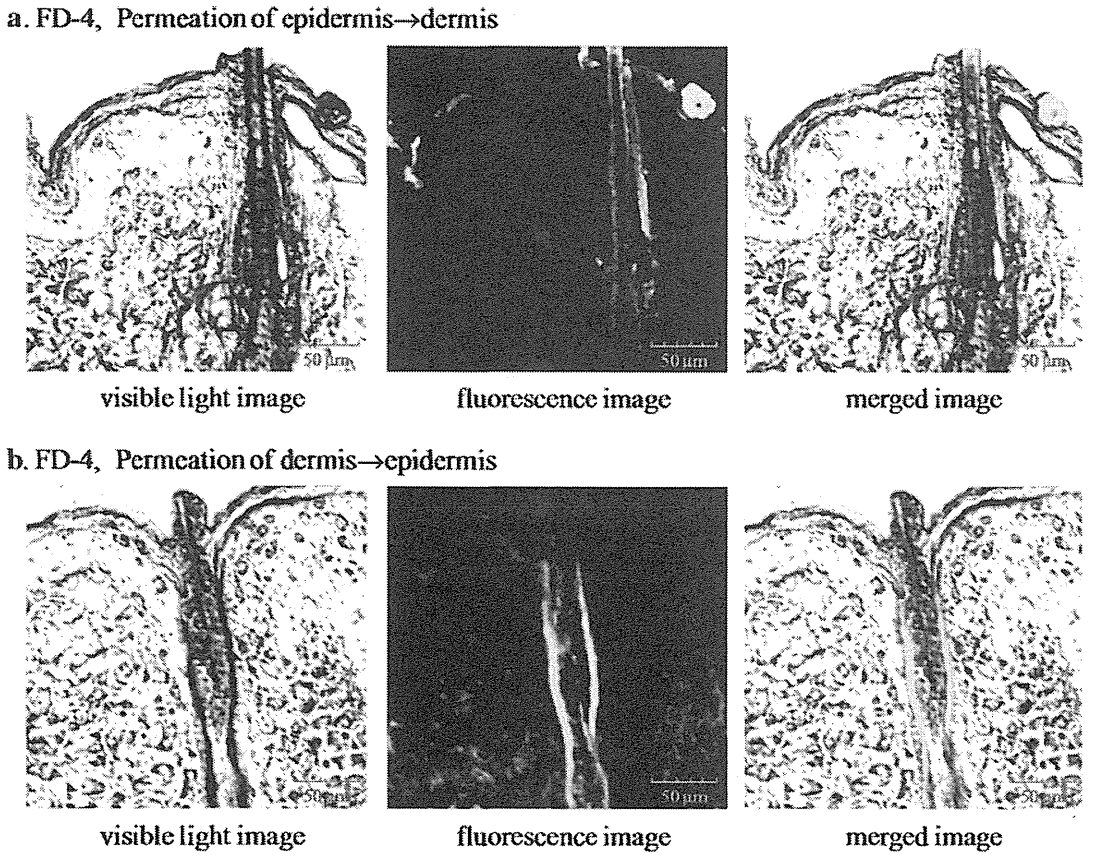

Fig. 8 Skin section image after the permeation experiment in epidermis-to-dermis (**a**) and dermis-to-epidermis directions (**b**).

clear fluorescence was observed for dermis-to-epidermis permeation. Although the dermis-to-epidermis FD-4 permeation was lower than the epidermis-to-dermis permeation, the skin concentration after application to the dermis side was much higher than that after application to the epidermis. Compounds are permeated firstly through the stratum corneum with a high resistance in the epidermis-to-dermis permeation, whereas they are permeated firstly through the dermis with a low resistance in the case of dermis-to-epidermis permeation. Therefore, the skin concentration of compounds after application to the epidermis is different from that after application to the dermis.

ISMN permeation was similar to the FD-4 permeation. Thus, hydrophilic low-molecular-weight compounds also permeate through the hair follicles. The morphological difference between the epidermis side and the dermis side, especially for the vertical shape of hair follicles, results in the difference in the skin permeation between epidermis-to-dermis and dermis-to-epidermis directions.

Figure 9 shows a comparison of ISMN permeations through human skin. Scalp human skin was used because scalp is typical skin with many hair follicles. Only one skin piece was obtained in the present study (*i.e.*, $n=1$). The dermis-to-epidermis permeation of ISMN was lower than the epidermis-to-dermis permeation, which was similar to the results for the hairless rat skin.

DISCUSSION

Since the uppermost lipophilic skin layer, stratum corneum, is the biggest barrier to the permeation of compounds through skin, skin permeation of compounds increases with lipophilicity or $\log K_{o/w}$ (8,15,34–36). However, a further increase in $\log K_{o/w}$ to more than 4.1 decreases the skin permeability (15,37,38). An increase in lipophilicity from MP to PP in the present study showed higher permeability. On the other hand, a further increase in the lipophilicity from PP to BP decreased the permeability. In addition, the stripped skin permeability was lower than that of the full-thickness skin for PeP. Furthermore, the addition of ethanol at a concentration of 3% improved the unusual results for the PeP permeation. Interfacial resistance and unstirred layer may need to be taken into account, especially for the skin permeation of highly lipophilic compounds ($\log K_{o/w}$ of more than 4.1) such as PeP.

The diffusion of chemical compounds through a dissolution-diffusion membrane is greatly affected by their

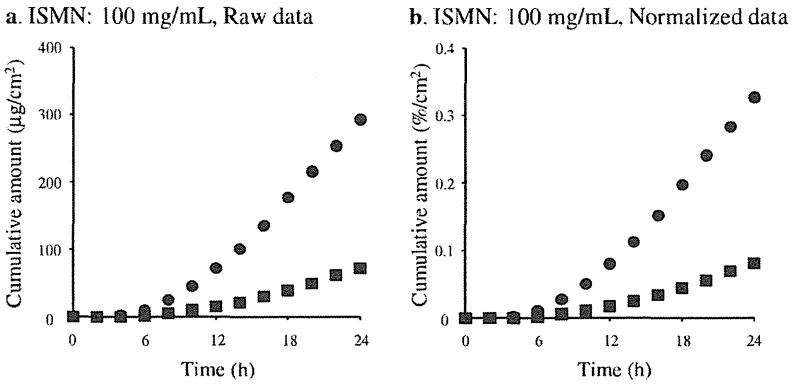

Fig. 9 Time course of changes in the cumulative amount of ISMN that permeated through human scalp skin from raw data (**a**) and normalized data (**b**). Symbols: as in Fig. 4 ($n=1$).

molecular sizes. In contrast, the distribution or partition from the donor solutions (vehicles) to the dissolution-diffusion membrane occurs rapidly, so the phenomena are not expressed by kinetics. This is well known in mass-transfer and rate process engineering (39,40). We thus used the concept of interfacial resistance to explain compound diffusion profiles from the matrices (20). No proof has been obtained as to why ethanol added to the formulations increased the skin permeation of highly lipophilic compounds. It has been proven, however, that ethanol decreases the interfacial resistance of highly lipophilic compounds between aqueous vehicles and skin (41–43). In other words, ethanol does not affect the diffusion of the compounds through the skin barrier.

Several penetrants may have adsorbed to the skin surface and diffusion cells. The adsorption took place in the epidermis-to-dermis permeation of MP for which $\log K_{o/w}$ is 1.9. The final concentration in addition to the initial concentration of penetrants must be determined to understand the real permeability. Only a few researchers are interested in dermis-to-epidermis permeation. However, comparison of epidermis-to-dermis permeation and dermis-to-epidermis permeation is very important to understand the mechanism

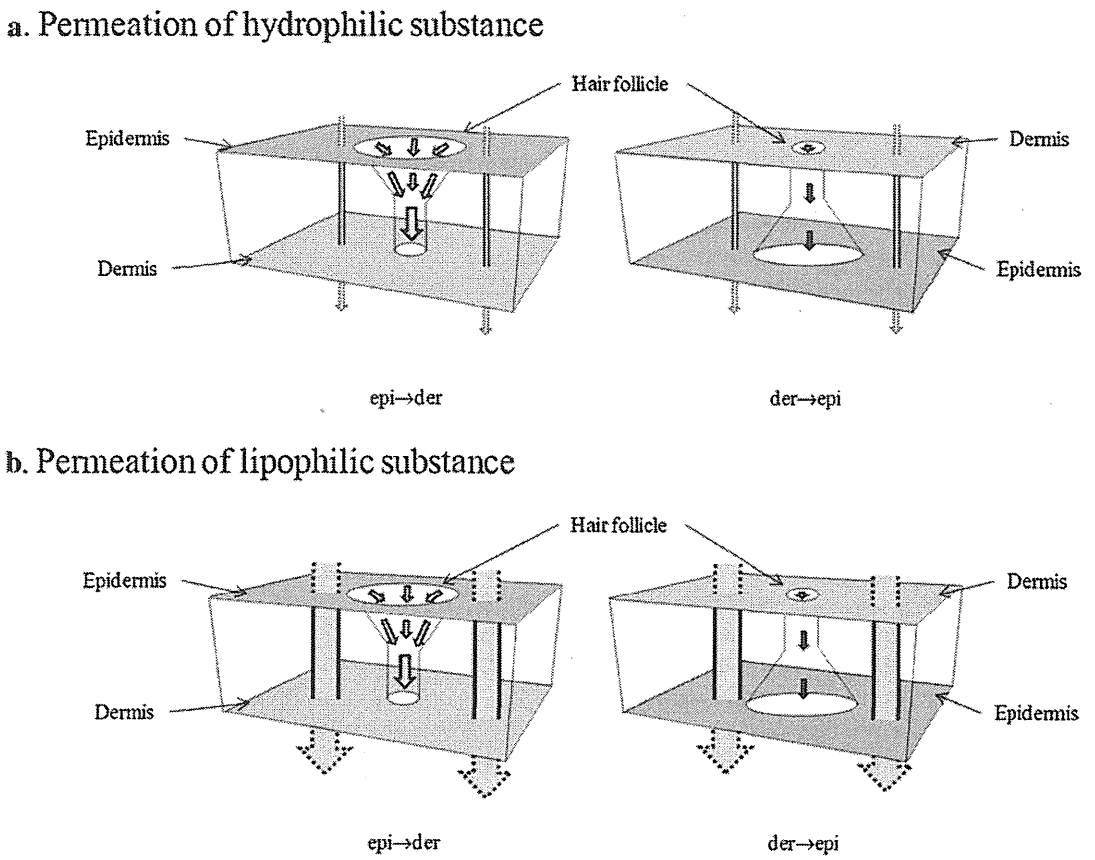

Fig. 10 Conical pore model of permeation pathway of hydrophilic compounds (**a**) and lipophilic compounds (**b**) through skin.

of skin permeation of compounds. Analysis of the adsorption of compounds is also very important. Since compounds with $\log K_{o/w}$ of about 2 are usually taken up by the skin surface, these compounds may easily adsorb to the skin.

In the case of aqueous penetrants, however, the epidermis-to-dermis permeability was higher than the dermis-to-epidermis permeability, even when modification was carried out using the final donor concentration. No or little skin permeation was observed when the molecular weight of penetrants was more than 500 Da (32). When determined in detail, scarce skin permeation was sometimes observed, even using penetrants larger than 500 Da. This is probably due to the hair follicles or other pore pathways (27,44–50). Trans-appendage routes containing the trans-follicular routes must be considered to fully understand the skin permeation profiles.

Among the compounds used in this experiment, the epidermis-to-dermis permeations of FD-4 and ISMN through full-thickness skin were different from the dermis-to-epidermis permeations. In the permeation through stripped skin, however, no effect of direction was found on the skin permeation of both hydrophilic compounds and lipophilic compounds. These findings suggest that the effect of direction on the skin permeations of FD-4 and ISMN is closely related to the vertical morphology of the stratum corneum. Figure 10 shows a schematic illustration of permeation through stratum corneum of hydrophilic compounds and lipophilic compounds. As shown in the figure, the apertural area of the appendage is largely open, and the appendage is narrower at the deeper site, suggesting a conical shape of pore for the appendage. In the case of epidermis-to-dermis permeation, the donor solution is easily approached to the large pore, resulting in the high partitioning of the penetrants into skin. When the donor solution was applied to a membrane having large pores, the compound molecules in solution contacted to large pores are easily penetrated into the pores. In contrast, in the case of dermis-to-epidermis permeation, donor solution is not easily approached to the appendage or is easily approached only to narrow appendages. Hydrophilic compounds probably permeate through the pore regions, not the real domain of the stratum corneum (Fig. 10a). Thus, the epidermis-to-dermis permeations of FD-4 and ISMN were higher than the dermis-to-epidermis permeations. Lipophilic compounds also permeate through the pore regions (Fig. 10b). The contribution of pore regions, however, is very low for the skin permeation of lipophilic compounds since the area ratio of the pore is only 0.1%.

CONCLUSION

Skin permeation profiles of high lipophilic compounds (*i.e.*, PcP) and aqueous compounds (*i.e.*, FD-4 and ISMN) were not simply explained by Fick's law of diffusion as follows: the stripped skin permeability of PcP was lower than full-thickness skin permeabilities, and the epidermis-to-dermis permeations of FD-4 and ISMN were higher than those in the opposite direction. Interfacial permeation resistance, adsorption of compounds on the skin surface and conical shape (or infundibulum) of hair follicles must be taken into account to fully understand these skin permeation profiles and mechanism involved. The present observation can be utilized to analyze transport pathway and mechanism of many penetrants through skin.

REFERENCES

1. Takeuchi H, Terasaka S, Sakurai T, Furuya A, Urano H, Sugibayashi K. Variation assessment for *in vitro* permeabilities through yucatan micropig skin. Biol Pharm Bull. 2011;34:555–61.
2. Kim MK, Lee CH, Kim DD. Skin permeation of testosterone and its ester derivatives in rats. J Pharm Pharmacol. 2000;52:369–75.
3. Obata Y, Sato H, Li CJ, Takayama K, Higashiyama K, Nagai T, Isawa K. Effect of synthesized cyclohexanol derivatives using l-menthol as a lead compound on the percutaneous absorption of ketoprofen. Int J Pharm. 2000;198:191–200.
4. Pagliara A, Reist M, Geinoz S, Carrupt PA, Testa B. Evaluation and prediction of drug permeation. J Pharm Pharmacol. 1999;51:1339–57.
5. Morimoto Y, Hatanaka T, Sugibayashi K, Omiya H. Prediction of skin permeability of drug: comparison of human and hairless rat skin. J Pharm Pharmacol. 1992;44:634–9.
6. Wilk W, Grune-Wolff B. Validity of alternatives to animal experimentation in biomedical research. Cah Anesthesiol. 1990;38:203–6.
7. Priborsky J, Muhlbachov E. Evaluation of *in-vitro* percutaneous absorption across human skin and in animal models. J Pharm Pharmacol. 1990;42:468–72.
8. Hatanaka T, Inuma M, Sugibayashi K, Morimoto Y. Prediction of skin permeability of drugs. I. Comparison with artificial membrane. Chem Pharm Bull. 1990;38:3452–9.
9. Sugibayashi K, Todo H, Oshizaka T, Owada Y. Mathematical model to predict skin concentration of drugs: toward utilization of silicone membrane to predict skin concentration of drugs as an animal testing alternative. Pharm Res. 2010;27:134–42.
10. Moser K, Kriwet K, Naik A, Kalia YN, Guy RH. Passive skin penetration enhancement and its quantification *in vitro*. Eur J Pharm Biopharm. 2001;52:103–12.
11. Elias PM. Epidermal lipids, barrier function, and desquamation. J Invest Dermatol. 1983;80:44–9.
12. Downing DT. Lipid and protein structures in the permeability barrier of mammalian epidermis. J Lipid Res. 1992;33:301–13.
13. Williams AC, Barry BW. Skin absorption enhancers. Crit Rev Ther Drug Carrier Sys. 1992;9:305–53.
14. Higuchi T. Physical chemical analysis of percutaneous absorption process from creams and ointments. J Soc Cosmet Chem. 1960;11:85–97.
15. Yamaguchi K, Mitsui T, Aso Y, Sugibayashi K. Structure-permeability relationship analysis of the permeation barrier properties of the stratum corneum and viable epidermis/dermis of rat skin. J Pharm Sci. 2008;97:4391–403.
16. Meidan VM, Pritchard D. A two-layer diffusion model for describing the variability of transdermal drug permeation. Eur J Pharm Biopharm. 2010;74:513–7.
17. Tamura M, Sueishi T, Sugibayashi K, Morimoto Y, Juni K, Hasegawa T, Kawaguchi T. Metabolism of testosterone and its

ester derivatives in organotypic coculture of human dermal fibroblasts with differentiated epidermis. Int J Pharm. 1996;131:263–71.
18. Ahmed S, Imai T, Otagiri M. Evaluation of stereoselective transdermal transport and concurrent cutaneous hydrolysis of several ester prodrugs of propranolol: mechanism of stereoselective permeation. Pharm Res. 1996;13:1524–9.
19. Sugibayashi K, Hayashi T, Matsumoto K, Hasegawa T. Utility of a three-dimensional cultured human skin model as a tool to evaluate the simultaneous diffusion and metabolism of ethyl nicotinate in skin. Drug Metabol Pharmacokin. 2004;19:352–62.
20. Kokubo T, Sugibayashi K, Morimoto Y. Mathematical models describing the drug release kinetics from pressure sensitive adhesive matrix. J Contr Release. 1992;20:3–12.
21. Anissimov YG, Roberts MS. Diffusion modeling of percutaneous absorption kinetics: 2. Finite vehicle volume and solvent deposited solids. J Pharm Sci. 2001;90:504–20.
22. Hadgraft J, Ridout G. Development of model membranes for percutaneous absorption measurements. I. Isopropyl myristate. Int J Phram. 1987;39:149–56.
23. Albery WJ, Burke JF, Leffler EB, Hadgraft J. Interfacial transfer studied with a rotating diffusion cell. J C S Faraday Trans I. 1976;72:1618–28.
24. Hadgraft J. Calculations of drug release rates from controlled release devices. The slab. Int J Pharm. 1979;2:177–94.
25. Tojo K. Hydrodynamic characteristics of an *in vitro* drug permeation cell. Ind Eng Chem Fundamen. 1985;24:368–73.
26. Henning A, Schaefer UF, Neumann D. Potential pitfalls in skin permeation experiments: influence of experimental factors and subsequent data evaluation. Eur J Pharm Biopharm. 2009;72:324–31.
27. Scheuplein RJ. Mechanism of percutaneous absorption. II. Transient diffusion and the relative importance of various routes of skin penetration. J Invest Dermatol. 1967;48:79–88.
28. Li Q, Tsuji H, Kato Y, Sai Y, Kubo Y, Tsuji A. Characterization of the transdermal transport of flurbiprofen and indomethacin. J Contr Release. 2006;110:542–56.
29. Ito K, Kato Y, Tsuji H, Nguyen HT, Kubo Y, Tsuji A. Involvement of organic anion transport system in transdermal absorption of flurbiprofen. J Contr Release. 2007;124:60–8.
30. Sugibayashi K, Hosoya K, Morimoto Y, Higuchi WI. Effect of the absorption enhancer, Azone, on the transport of 5-fluorouracil across hairless rat skin. J Pharm Pharmacol. 1985;37:578–80.
31. Morimoto Y, Sugibayashi K, Hosoya K, Higuchi WI. Penetration enhancer effect of Azone on the transport of 5-fluorouracil across hairless rat skin. Int J Pharm. 1986;32:31–8.
32. Bos JD, Meinardi MM. The 500 dalton rule for the skin penetration of chemical compounds and drugs. Exp Dermatol. 2000;9:165–9.
33. Todo H, Kimura E, Yasuno H, Tokudome Y, Hashimoto F, Sugibayashi K. Permeation pathway of macromolecules and nanospheres through skin. Biol Pharm Bull. 2010;33:1394–9.
34. Potts RO, Guy RH. Predicting skin permeability. Pharm Res. 1992;9:663–9.
35. Flynn GL, Yalkowsky SH. Correlation and prediction of mass transport across membranes I: influence of alkyl chain length on flux-determining properties of barrier and diffusant. J Pharm Sci. 1972;61:838–52.
36. Lien EJ, Gao H. QSAR analysis of skin permeability of various drugs in man as compared to *in vivo* and *in vitro* studies in rodents. Pharm Res. 1995;12:583–7.
37. Yano T, Nakagawa A, Tsuji M, Noda K. Skin permeability of various non-steroidal anti-inflammatory drugs in man. Life Sci. 1986;39:1043–50.
38. Scheuplein RJ, Blank IH, Brauner GJ, MacFarlane DJ. Percutaneous absorption of steroids. J Invest Dermatol. 1969;52:63–70.
39. Quinn JA, Jeanin PG. Interfacial resistance: diffusion into a laminar liquid-liquid jet. Chem Eng Sci. 1961;15:243–50.
40. Scott EJ, Tung LH, Drickamer HG. Diffusion through an interface. J Chem Phys. 1951;19:1075–8.
41. Sugibayashi K, Nemoto M, Morimoto Y. Effect of several penetration enhancers on the percutaneous absorption Indomethacin in hairless rats. Chem Pharm Bull. 1988;36:1519–28.
42. Kim YC, Park JH, Ludovice PJ, Prausnitz MR. Synergistic enhancement of skin permeability by N-lauroylsarcosine and ethanol. Int J Pharm. 2008;352:129–38.
43. Suhonen TM, Bouwstra JA, Urtti A. Chemical enhancement of percutaneous absorption in relation to stratum corneum structural alterations. J Control Release. 1999;59:149–61.
44. Du Plessis J, Egbaria K, Ramachandran C, Weiner ND. Topical delivery of liposomally encapsulated gamma-interferon. Antiviral Res. 1992;18:259–65.
45. Feldmann JR, Maibach HI. Regional variation in percutaneous penetration of 14 C cortisol in man. J Invest Dermatol. 1967; 48:181–3.
46. Maibach HI, Feldmann JR, Hilby TH, Serat WF. Regional variation in percutaneous penetration in man. Pesticides Arch Environ Health. 1971;23:208–11.
47. Illel B. Formulation for transfollicular drug administration: some recent advances. Crit Rev Ther Drug Carrier Syst. 1997;14:207–19.
48. Wosicka H, Cal K. Targeting to the hair follicles: current status and potential. J Dermatol Sci. 2010;57:83–9.
49. Lauer AC, Lieb LL, Ramachandran C, Flynn GL, Weiner ND. Transfollicular drug delivery. Pharm Res. 1995;12:179–86.
50. Ramachandran C, Fleisher D. Transdermal delivery of drug for the treatment of bone diseases. Adv Drug Deliv Rev. 2000;42:197–223.

Pharm Res
DOI 10.1007/s11095-013-0997-4

RESEARCH PAPER

Inhalable Powder Formulation of Pirfenidone with Reduced Phototoxic Risk for Treatment of Pulmonary Fibrosis

Satomi Onoue • Yoshiki Seto • Masashi Kato • Yosuke Aoki • Yoshiki Kojo • Shizuo Yamada

Received: 18 September 2012 / Accepted: 28 January 2013

ABSTRACT

Purpose Orally-taken pirfenidone (PFD), an idiopathic pulmonary fibrosis drug, often causes severe phototoxicity. Present study aimed to develop a respirable powder formulation for PFD (PFD-RP) to minimize phototoxic risk.

Methods Photochemical properties of PFD were examined using a reactive oxygen species (ROS) assay and photostability testing. PFD-RP was characterized with a focus on photostability, *in vitro* inhalation performance, and the efficacy in antigen-sensitized rats. Pharmacokinetic studies were conducted after oral and intratracheal administration of PFD formulations.

Results Although PFD solution exhibited photodegradation under simulated sunlight (250 W/m^2), both PFD powder and PFD-RP were photochemically stable. Laser diffraction and cascade impactor analyses on PFD-RP suggested its high dispersion and fine *in vitro* inhalation performance. Inhaled PFD-RP (300 μg-PFD/rat) could suppress antigen-evoked pulmonary inflammation in rats as evidenced by decreases in recruited inflammatory cells and neutrophilia-related biomarkers in the lung. Exposure of PFD to light-exposed tissues (skin and eye) after intratracheal administration of PFD-RP at a pharmacologically effective dose (300 μg-PFD/rat) was 90–130-fold less than that of the oral PFD dosage form at a phototoxic dose (160 mg/kg).

Conclusions PFD-RP might be an attractive alternative to the current oral PFD therapy with a better safety margin.

KEY WORDS inhalation · photostability · phototoxicity · pirfenidone · pulmonary fibrosis

S. Onoue (✉) · Y. Seto · M. Kato · Y. Aoki · Y. Kojo · S. Yamada
Department of Pharmacokinetics and Pharmacodynamics
School of Pharmaceutical Sciences
University of Shizuoka, 52-1 Yada, Suruga-ku
Shizuoka 422-8526, Japan
e-mail: onoue@u-shizuoka-ken.ac.jp

Published online: 21 February 2013

ABBREVIATIONS

8-MOP	8-methoxypsoralen
ANOVA	analysis of variance
AUC	area under concentration *versus* time curve
AUMC	area under moment curve
BALF	bronchoalveolar lavage fluid
EPO	eosinophil peroxidase
ESI-MS	electrospray ionization mass spectrometry
FQ	fluoroquinolones
HPMC	hydroxypropyl methylcellulose
MPO	myeloperoxidase
MRT	mean residence time
OVA	ovalbumin
PBS	phosphate-buffered saline
ROS	reactive oxygen species
RP	respirable powder
SEM	scanning electron microscopy
TMBZ	3,3′,5,5′-tetramethylbenzidine
UPLC	ultra performance liquid chromatography

INTRODUCTION

Pirfenidone (PFD), 5-methyl-1-phenylpyridin-2-one, is a novel anti-fibrotic and anti-inflammatory agent for suppressing the progression of lung, kidney, and hepatic fibrosis and inflammatory events in experimental animal models (1–4). PFD can regulate the activity of TGF-β and TNF-α, leading to the inhibition of fibroblast proliferation and collagen synthesis (5). The detailed mechanism whereby PFD modulates fibrogenesis is still unclear and the biological activities of PFD may be multitargeted. PFD has been clinically used as the first anti-fibrotic drug (Esbriet®, Pirespa®) available for mild-to-moderate idiopathic pulmonary fibrosis (IPF) in Europe, Japan, India, and China (4,6,7). Although PFD

has an attractive therapeutic potential for the treatment of IPF, orally-taken PFD often causes systemic side effects, such as nausea, anorexia, dizziness, rash, hepatic dysfunction, and phototoxicity (6,8,9). In particular, the phototoxic skin response is a well-known adverse effect of PFD treatment and its frequency has been shown to be as much as ca. 50% in a clinical study (8). PFD-induced phototoxicity may be controlled by either dose reductions or the termination of treatment; however, in the clinical study, there were no significant differences in the incidence of phototoxicity between the high-dose (51% in patients with 1.8 g/day of PFD) and low-dose group (53% in patients with 1.2 g/day of PFD).

Phototoxic skin responses can be caused by the combined effects of UV/VIS irradiation and external phototoxic drugs (10), and increasing attention has been drawn to drug-induced phototoxicity because of the gradual expansion of the UV portion in the solar spectrum. Owing to possible reductions in medication compliance, drug-induced phototoxicity is one of the impediments in pharmaceutical development and a number of efforts have been made to avoid drug-induced phototoxic reactions. Theoretically, drug-induced phototoxicity is induced in light-exposed tissues, especially skin (11,12); therefore, control of dermal PFD concentrations with use of appropriate formulation technologies may be of great value for reducing the phototoxic risk of PFD. Recently, several respirable formulation systems have been developed for the treatment of airway inflammation and inhalation therapy could achieve a high drug concentration in the lung with low systemic exposure (13,14). Strategic application of PFD to the respirable formulation system may also lead to successful development of efficacious PFD medications with a wide safety margin, whereas far less is known about the feasibility and pharmacological outcomes of the respirable formulation of PFD.

The present study aimed to design a new respirable formulation system for PFD with the aim of maximizing topical effects in the lung and minimizing the exposure of PFD to light-exposed tissues. Based on results from photostability testing on PFD samples, the respirable powder (RP) formulation of PFD, composed of lactose carriers and a micronized mixture of PFD and erythritol, was developed with a jet mill. The physicochemical properties of PFD-RP were characterized with a focus on morphology by scanning electron microscopy, particle size distribution by laser diffraction analysis, and *in vitro* inhalation performance by cascade impactor experiments. In antigen-sensitized rats, the pharmacological effects of insufflated PFD-RP were assessed upon recruitment of inflammatory cells and neutrophilia-/eosinophilia-related biomarkers in bronchoalveolar lavage fluid (BALF). To verify the photosafety of PFD-RP, comparative pharmacokinetic studies were carried out in rats after intratracheal administration of PFD-RP at pharmacologically effective doses or oral administration of PFD at phototoxic and non-phototoxic doses.

MATERIALS AND METHODS

Chemicals

PFD was kindly provided by Shionogi (Osaka, Japan). Respitose® SV-003 and erythritol were supplied by DMV (Veghel, The Netherlands) and Nikken Chemicals (Tokyo, Japan), respectively. Aluminum hydroxide (alum) gel, horseradish peroxidase, ovalbumin (OVA), and sodium pentobarbital were purchased from Sigma Aldrich (St. Louis, MO). Ammonium acetate, *o*-phenylenediamine (OPD), and trypan blue were bought from Wako Pure Chemical Industries (Tokyo, Japan). 3,3′,5,5′-Tetramethylbenzidine (TMBZ) was bought from Dojindo (Kumamoto, Japan). All other reagents were obtained from commercial sources.

Solar Simulator

Photochemical studies were carried out using an Atlas Suntest CPS+ solar simulator (Atlas Material Technology LLC, Chicago, IL, USA) equipped with a xenon arc lamp (1,500 W). A UV special filter was installed to adapt the spectrum of the artificial light source to that of natural daylight. An irradiation test was carried out at 25°C with an irradiance of 250 W/m^2 (300–800 nm).

Reactive Oxygen Species (ROS) Assay

The ROS assay was originally designed to evaluate the photochemical reactivity of tested chemicals by determining both singlet oxygen and superoxide generated from photo-irradiated chemicals (15). In the present study, the ROS assay was undertaken to clarify the photochemical properties of PFD. Briefly, singlet oxygen was measured in an aqueous solution by spectrophotometrically monitoring the bleaching of RNO at 440 nm using imidazole as a selective acceptor of singlet oxygen. Samples, containing the tested chemical (200 μM), *p*-nitrosodimethylaniline (50 μM), and imidazole (50 μM) in 20 mM sodium phosphate buffer (NaPB) (pH 7.4), were irradiated with simulated sunlight (250 W/m^2) and then UV absorption at 440 nm was measured using a SAFIRE microplate spectrophotometer (TECAN, Männedorf, Switzerland). For the determination of superoxide, samples containing the tested chemical (200 μM) and

nitroblue tetrazolium (NBT, 50 μM) in 20 mM NaPB were irradiated with simulated sunlight for 1 h and reductions in NBT were measured by increases in absorbance at 560 nm using a SAFIRE microplate spectrophotometer (TECAN).

Photostability Testing

For the solid-state stability test, PFD formulations (5 mg) were weighed exactly and spread in a 15 mL clear glass vial over the whole bottom surface. For the solution-state stability study, PFD (5 mg) was weighed in a 15 mL clear glass vial and dissolved in 5 mL of distilled water. Each sample was set in the Suntest CPS+ solar simulator and irradiated with simulated sunlight (250 W/m^2) for the indicated periods. A reference sample protected by aluminum foil was examined under the same conditions. Each solid sample was dissolved in 10 mL of 50% acetonitrile and PFD remaining in the sample was determined with ultra-performance liquid chromatography equipped with electrospray ionization mass spectrometry (UPLC/ESI-MS) analysis. The UPLC/ESI-MS system consisted of a Waters Acquity UPLC^{TM} system (Waters), which included a binary solvent manager, a sample manager, a column compartment, and a Micromass SQ detector connected with Waters MassLynx v 4.1. A Waters Acquity UPLC^{TM} BEH C_{18} (particle size: 1.7 μm, column size: Φ 2.1×50 mm; Waters) was used and column temperature was maintained at 40°C. Samples were separated using a gradient mobile phase consisting of Milli-Q containing 0.1% formic acid (A) and MeOH (B). The gradient condition of the mobile phase was 0–0.5 min, 80% A; 0.5–4 min, 80–25% A (gradient curve: 8); 4–5 min, 5% A; 5–6 min, 80% A, and the flow rate was set at 0.25 mL/min. Analysis was carried out using SIR for specific m/z: 186 $[M+H]^+$ for PFD.

Preparation of Respirable Powder Formulations

RP formulations of PFD and OVA (PFD-RP and OVA-RP) were prepared as reported previously (14). PFD or OVA particles and excipients, including lactose or erythritol, respectively, were first ground to fine powders with a pestle and mortar and then milled with an A-O JET MILL (Seishin Enterprise, Tokyo, Japan) at a pusher nozzle pressure and grinding nozzle pressure of 6.0 and 6.5 kg/cm^{2}G for PFD or 6.0 and 5.5 kg/cm^{2}G for OVA, respectively. The ratio of PFD or OVA to excipient was 3:2 or 1:400 (w/w), respectively. Micronized PFD and OVA were decompounded with 10-fold lactose (Respitose®, SV-003) and erythritol carrier particles, respectively, in a plastic bag for 3 min and the obtained dry powders of PFD and OVA were stored in a vacuum desiccator until tested. The amount of PFD in the RP formulation was determined by UPLC/ESI-MS analysis as described in the "Photostability Testing" section.

Scanning Electron Microscopy (SEM)

PFD-RP was coated with platinum on a HITACHI Ion Sputter E-1010 (Hitachi, Tokyo, Japan). Representative scanning electron microscopic images of PFD-RP were taken using a VE-7800 scanning electron microscope (Keyence Corporation, Osaka, Japan). For SEM observations, each sample was fixed on an aluminum sample holder using double-sided carbon tape.

Particle Size Distribution

The particle size distribution of PFD-RP was measured using a laser diffraction scattering method with an LMS-2000e (Seishin Enterprise, Tokyo, Japan). PFD-RP was subjected to dry spraying at a pressure of 0.2 MPa for effective dispersion into fine particles and carrier molecules and then particles were calculated.

Cascade Impactor Analysis

The *in vitro* inhalation performance of the RP formulation was assessed according to USP 29 <601> AEROSOLS using an AN-200 system (Shibata Scientific Technology, Tokyo, Japan), consisting of a vacuum pump, mass flow meter, and eight-stage Andersen cascade impactor. Briefly, dry powders were filled into a JP No. 2 hard capsule of hydroxypropyl methylcellulose (HPMC) and the capsule was installed in a JetHaler® (Hitachi Unisia, Kanagawa, Japan) powder inhaler. Dry powder formulations (40 mg) in each capsule were dispersed *via* the device with an inspiration rate of 28.3 L/min for an inhalation time of 10 s×5 times and the collection stages of the impactor (stages 0–7) were washed with purified water. PFD in each solution was determined by UPLC/ESI-MS as described in the "Photostability Testing" section. The fine particle dose (FPD) was defined as the mass of drug particles measuring less than 5.8 μm (particles deposited at stage 2 and lower). The fine particle fraction (FPF) was calculated as the ratio of FPD to the total loaded dose.

Animals and Drug Insufflation

Male Sprague–Dawley rats (7–9 weeks of age; Japan SLC, Shizuoka, Japan), weighing 200–350 g, were housed three per cage in the laboratory with free access to food and water and were maintained on a 12-h dark/light cycle in a room with controlled temperature (24±1°C) and humidity (55±5%).

Animals were fasted for 12 h before experiments. Rats were sensitized by intraperitoneal injection of 100 μg of OVA with 5 mg of alum on days 0, 7, and 14. They were anesthetized with sodium pentobarbital (50 mg/kg, i.p.) and received intratracheal administration of OVA (100 μg/rat) powder at 24 h after the last OVA sensitization. At 1 h before the OVA challenge, PFD-RP (30–1,000 μg-PFD/kg) or PFD-free RP formulation (control-RP) was administered *via* intratracheal insufflation using a PennCentury insufflation powder delivery device (DP-4, INA Research Inc., Nagoya, Japan). A bolus (2 mL) of air from an attached syringe was used to deliver the preloaded powder from the chamber of the insufflator into the airway system of the rats. At 24 h after OVA challenge, rats were exsanguinated *via* the descending aorta under anesthesia with sodium pentobarbital and the lungs were perfused with 30 mL of saline and removed. All procedures used in the present study were conducted in accordance with the guidelines approved by the Institutional Animal Care and Ethical Committee of the University of Shizuoka.

Total Cell Counting in BALF

At 24 h after the OVA challenge, bronchoalveolar lavage fluid (BALF) was collected by washing the airways twice with 5 mL of PBS. BALF was pooled and immediately centrifuged at 112×*g* for 10 min, the supernatant was then removed, and cells were re-suspended with 1 mL of PBS. The total number of cells in BALF upon adding an equal amount of 0.2% trypan blue was counted using a Burker-Turk counting chamber.

Measurement of MPO and EPO Activities

Enzymatic detection of MPO and EPO in BALF was performed in accordance with a previous report (13,16). Briefly, for the MPO measurement, assay mixtures consisted of 40 μL of H_2O_2 (final concentration 0.3 mM) in 80 mM sodium phosphate buffer (pH 5.4) and 50 μL of BALF samples. The reaction was initiated by the addition of 10 μL of TMBZ (final concentration 1.6 mM) in dimethyl sulfoxide at 37°C and stopped after 2 min by the addition of 0.18 M H_2SO_4. Subsequently, optical density was determined at 450 nm. For the detection of EPO activity in BALF, the reaction mixture was prepared by adding 500 μL of OPD (50 mM) to 24.25 mL of Tris buffer (pH8.0), 3 μL of 30% H_2O_2, and 25 μL of Triton X-100. Then, 100 μL of reaction mixture was added to 50 μL of BALF sample in a 96-well plate and incubated for 30 min at room temperature. The reaction was stopped by the addition of 2 M H_2SO_4 and absorbance at 490 nm was measured. A titration curve of horseradish peroxidase was used for the calculation of MPO and EPO activities, which were expressed in arbitrary units. All samples were assayed in duplicate and optical densities in all assays were measured using a Safire microplate reader (Tecan).

Plasma Concentration of PFD After Oral Administration

Rats were anesthetized using pentobarbital (40 mg/kg, i.p.) and a cannula (PE8050, Natsume, Tokyo, Japan) was inserted into the arteria femoralis before PFD was administered orally. Blood samples (approximately 150 μL) were collected from the cannulated arteria femoralis at the indicated times (5, 10, 15, 30, 45 min, 1, 1.5, 2, 3, 4, and 6 h) after oral administration of PFD (30 and 160 mg/kg) or intratracheal administration of PFD-RP (300 μg-PFD/rat). Plasma obtained by centrifugation (10,000×*g*, 10 min, 4°C) was deproteinized by the addition of acetonitrile (plasma : acetonitrile = 2 : 5), and plasma was mixed and centrifuged (2,000 rpm, 1 min, 4°C). Supernatants were filtered and 50% acetonitrile solution containing antipyrine (5 μg/mL), an internal standard, was added (supernatant : nalidixic acid = 9 : 1) for UPLC/ESI-MS analysis as described in the "Photostability Testing" section.

Tissue Deposition of PFD

After oral administration of PFD (30 and 160 mg/kg) or intratracheal administration of PFD-RP (300 μg-PFD/rat), rats were sacrificed at the indicated periods (5, 30 min, 1, 2, 3, 4, and 6 h) by taking blood from the descending aorta under temporary anesthesia with diethyl ether and tissues were then perfused with cold saline from the aorta. The skin, lung, and eyes were dissected and fat and blood vessels were removed by trimming. Tissues were minced with scissors in stoppered test tubes and homogenized by a Cryo-press (CP-100W, Microtech, Chiba, Japan) and Physcotron (Microtech) in 4 mL of acetonitrile. After shaking for 5 min and sonication for 10 min, mixtures were centrifuged (3,000 rpm, 10 min). This extraction was repeated two times with acetonitrile and supernatants were pooled. Samples were evaporated to dryness under a gentle stream of nitrogen at 45°C and residues were dissolved in 50% acetonitrile solution containing antipyrine (500 ng/mL) as an internal standard for UPLC/ESI-MS analysis.

Pharmacokinetic Analysis

Pharmacokinetic characterization in plasma was performed by non-compartmental analysis as implemented in WinNonlin Professional Version 5.2 (Pharsight Corporation,